Structure of α-Glycerophosphate Oxidase from *Streptococcus* sp.: A Template for the Mitochondrial α-Glycerophosphate Dehydrogenase[†,‡]

Timothy Colussi,[§] Derek Parsonage,[§] William Boles,[§] Takeshi Matsuoka,[∥] T. Conn Mallett,[§,⊥] P. Andrew Karplus,[@] and Al Claiborne*[,§]

Center for Structural Biology, Wake Forest University School of Medicine, Winston-Salem, North Carolina 27157, Diagnostics Department, Asahi Kasei Pharma, Shizuoka 410-2321, Japan, and Department of Biochemistry and Biophysics, Oregon State University, Corvallis, Oregon 97331

Received August 20, 2007; Revised Manuscript Received October 2, 2007

ABSTRACT: The FAD-dependent α-glycerophosphate oxidase (GlpO) from *Enterococcus casseliflavus* and *Streptococcus* sp. was originally studied as a soluble flavoprotein oxidase; surprisingly, the GlpO sequence is 30−43% identical to those of the α-glycerophosphate dehydrogenases (GlpDs) from mitochondrial and bacterial sources. The structure of a deletion mutant of *Streptococcus* sp. GlpO (GlpOΔ, lacking a 50-residue insert that includes a flexible surface region) has been determined using multiwavelength anomalous dispersion data and refined at 2.3 Å resolution. Using the GlpOΔ structure as a search model, we have also determined the intact GlpO structure, as refined at 2.4 Å resolution. The first two domains of the GlpO fold are most closely related to those of the flavoprotein glycine oxidase, where they function in FAD binding and substrate binding, respectively; the GlpO C-terminal domain consists of two helix bundles and is not closely related to any known structure. The flexible surface region in intact GlpO corresponds to a segment of missing electron density that links the substrate-binding domain to a ββα element of the FAD-binding domain. In accordance with earlier biochemical studies (stabilizations of the covalent FAD-N5−sulfite adduct and *p*-quinonoid form of 8-mercapto-FAD), Ile430-N, Thr431-N, and Thr431-OG are hydrogen bonded to FAD-O2α in GlpOΔ, stabilizing the negative charge in these two modified flavins and facilitating transfer of a hydride to FAD-N5 (from Glp) as well. Active-site overlays with the glycine oxidase−*N*-acetylglycine and D-amino acid oxidase−D-alanine complexes demonstrate that Arg346 of GlpOΔ is structurally equivalent to Arg302 and Arg285, respectively; in both cases, these residues interact directly with the amino acid substrate or inhibitor carboxylate. The structural and functional divergence between GlpO and the bacterial and mitochondrial GlpDs is also discussed.

The FAD-linked oxidation of α-glycerophosphate (Glp)[1] to DHAP occurs in at least three contexts. The first two are α-glycerophosphate dehydrogenases (GlpDs) from mitochondria [*mito*GlpD (*1*−*4*)] and from bacteria [*bact*GlpD (*5*, *6*)], clearly homologous enzymes having sequences that are ca. 30−33% identical. The third FAD-dependent Glp-oxidizing enzyme is α-glycerophosphate oxidase (GlpO), found predominantly (if not exclusively) in heme-deficient lactic acid bacteria such as *Enterococcus casseliflavus* [formerly *Streptococcus faecium* (*7*, *8*)]. GlpOs are homologous with the *bact*- and *mito*GlpDs, having sequences 30−43% identical with them but being distinguished by a ca. 50-residue insert falling between two segments proposed by sequence to interact with the Glp substrate (*9*). The *mito*GlpD is an important component of the Glp shuttle that serves to transfer NADH-derived reducing equivalents from the cytosol to the mitochondrion (*10*). Mammalian *mito*GlpD has also been implicated in insulin signaling (*11*, *12*) and differs from yeast *mito*GlpD and *bact*GlpDs in that it has a C-terminal ca. 100-residue extension that is homologous to calmodulin (*3*). Little is known of the structure and properties of the mammalian *mito*GlpD because of its extreme insolubility and the difficulty of purifying it in good yield and in an unmodified form (*2*, *13*). It has been localized to the outer surface of the inner mitochondrial membrane, with both the Glp substrate and $Fe(CN)_6^{3-}$ acceptor sites facing the intermembrane space (*14*).

[†] This work was supported by National Institutes of Health (NIH) Grant GM-35394 (A.C.) and by National Science Foundation Grant MCB-9982727 (P.A.K.). New data for this study were measured at beamline X26C of the National Synchrotron Light Source. Financial support comes principally from the Offices of Biological and Environmental Research and of Basic Energy Sciences of the U.S. Department of Energy and from the National Center for Research Resources of the National Institutes of Health.

[‡] Coordinates have been deposited with the Protein Data Bank as entries 2RGH and 2RGO.

* To whom correspondence should be addressed. Telephone: (336) 716-3914. Fax: (336) 777-3242. E-mail: alc@csb.wfu.edu.

[§] Wake Forest University School of Medicine.

[∥] Asahi Kasei Pharma.

[⊥] Present address: Rigaku, Sevenoaks, Kent TN15 6QY, England.

[@] Oregon State University.

[1] Abbreviations: Glp, L-α-glycerophosphate; DHAP, dihydroxyacetone phosphate; GlpD, α-glycerophosphate dehydrogenase (flavin-dependent); *mito*GlpD, mitochondrial α-glycerophosphate dehydrogenase; *bact*GlpD, bacterial α-glycerophosphate dehydrogenase; GlpO, α-glycerophosphate oxidase; DAAO, D-amino acid oxidase; E*, resting oxidized enzyme form that does not productively bind substrate; GlpOΔ, α-glycerophosphate oxidase deletion mutant lacking residues Asp356−Ala405; PCR, polymerase chain reaction; SeMet, selenomethionine; MAD, multiwavelength anomalous dispersion; ThiO, glycine oxidase; MSOX, monomeric sarcosine oxidase.

10.1021/bi701685u CCC: $40.75
Published on Web 12/23/2007

While all GlpDs are membrane-associated, it is unclear in some cases whether they are peripheral or integral membrane proteins. For instance, the mammalian *mito*GlpD has been localized to the outer surface of the inner membrane (*14*), but another analysis predicts it to be an integral membrane protein with three transmembrane helices (*4*). Similarly, *Escherichia coli* GlpD was reported to require detergent solubilization, leading to the conclusion that it was an integral membrane protein (*15*), but later a His-tagged version of *E. coli* GlpD was purified without detergent solubilization (*16*). Still another recent report referred to the *E. coli* GlpD as an integral membrane flavoenzyme with "six transmembrane spanning" regions (*17*). The *Bacillus subtilis* GlpD is found predominantly (~75%) in the cytosolic fraction following ultracentrifugation of an extract from glycerol-grown cells (*18*).

Functionally, GlpO differs from GlpD in its efficient catalytic reduction of O_2 to H_2O_2, with the *En. casseliflavus* enzyme having a $k_{cat}/K_m(O_2)$ of $\sim 10^6$ M^{-1} s^{-1} (*9*); also, GlpO is clearly a dimeric (*8*), cytosolic protein (*8, 19*). Because GlpO also exhibits "dehydrogenase" activities that are similar to those of *E. coli* GlpD (*8, 15*), with acceptor substrates such as $Fe(CN)_6^{3-}$, there is great potential for using the better-behaved GlpO as a structural and even functional template for the GlpDs. Studies of *En. casseliflavus* GlpO revealed an active-site environment similar to those of D-amino acid oxidase (DAAO) and other flavoprotein oxidases; the enzyme stabilizes the blue *p*-quinonoid form of 8-mercapto-FAD (*8*), it reacts reversibly with sulfite to form a covalent FAD−N5-adduct (*8*), and the apoprotein raises the redox potential of bound FAD by 100 mV relative to that of the free coenzyme (*9*). Stopped-flow analyses of the reductive half-reaction also indicate that the resting oxidized enzyme exists in two states (E and E*), only one of which productively binds Glp for reduction (*9*). A limited proteolysis study with *Streptococcus* sp. GlpO (*20*) demonstrated that the ca. 50-residue insert unique to the GlpOs was largely excised, with the nicked enzyme (40 and 23 kDa fragments remain associated) retaining catalytic activity with an ~20-fold increase in K_m(Glp) and an 8-fold decrease in k_{red}. Interestingly, whereas intact *Streptococcus* sp. GlpO has no E* form, for the nicked enzyme E* is near 50%.

The relative paucity of structural information for Glp recognition and binding together with its central role in an important mitochondrial shuttle and electron transport (*10*) led us to initiate a structural study of GlpO from *Streptococcus* sp. (*21*). Here, we report the crystal structures of both GlpOΔ, a GlpO deletion mutant lacking the 50-residue insert, and of intact GlpO, refined at 2.3 and 2.4 Å resolution, respectively. Of particular interest are the two respective active-site conformations, one of which appears to be unproductive for catalysis and may represent the E* state.

EXPERIMENTAL PROCEDURES

*Expression and Purification of GlpO*Δ. The *Streptococcus* sp. *glpO* gene (*20*), contained in a plasmid generously provided by Asahi Kasei Pharma, was amplified by PCR and cloned into pQE30 (Qiagen) to express the N-terminal His-tagged protein. The 3′-end of the gene was PCR-amplified using a primer bridging the required deletion in combination with a downstream primer. The resulting PCR product was purified and served as a primer, along with a primer from the 5′-end of the gene, for PCR of the entire *glpO*Δ coding sequence, which was then cloned into pQE30. After the gene had been sequenced to confirm both the required deletion and the absence of other mutations, the plasmid was transformed into *E. coli* B834 cells containing pREP4 (Qiagen) for expression of GlpOΔ. These cells were grown at 37 °C in a 3-L culture of MOPS-based defined medium (EZ Rich Defined Medium, Teknova) containing 25 μg/mL kanamycin and 100 μg/mL ampicillin, with GlpOΔ expression being induced by addition of 0.5 mM isopropyl-β-D-thiogalactopyranoside at an A_{600} of 0.9. After induction, the temperature was lowered to 25 °C, and growth was continued overnight. GlpOΔ was purified using a combination of Q-Sepharose and Ni-NTA columns as described by Nicely et al. (*22*), except that cells were lysed using an Aminco French press, and β-mercaptoethanol was omitted from the column buffers. Pure protein was buffer-exchanged into 50 mM potassium phosphate (pH 7.0) containing 1 mM EDTA and concentrated to 10 mg/mL before being frozen in aliquots at −70 °C. The SeMet protein was expressed and purified in the same way, but with SeMet replacing Met in the growth medium.

*Spectral Analyses of GlpO*Δ *and Stopped-Flow Kinetics.* Titrations with dithionite and sulfite and other static spectral measurements followed established protocols (*9, 20*), using an experimentally determined ϵ_{450} of 11 600 M^{-1} cm^{-1} for purified GlpOΔ. Steady-state kinetic parameters for GlpOΔ were determined in enzyme-monitored turnover experiments, carried out with the Applied Photophysics DX.17 MV stopped-flow spectrophotometer as described previously (*9, 20*). Kinetic data were analyzed as described by Cornish-Bowden (*23*), as follows.

$$v = Vab/(K_{iA}K_{mB} + K_{mB}a + K_{mA}b + ab)$$

where A and B represent Glp and O_2, respectively. Primary plots of b/v versus b intersect to the left of the y-axis in the case of an ordered ternary complex mechanism. A secondary plot of slope × a versus a gives a y-axis intercept of K_{mA}/V_{max} and has a slope equal to $1/V_{max}$. A secondary plot of intercept × a versus a gives a y-axis intercept of $K_{iA}K_{mB}/V_{max}$ and has a slope equal to K_{mB}/V_{max}.

Crystallization and Data Collection. Purification, crystallization, and data collection for native intact *Streptococcus* sp. GlpO have been described in previous reports (*20, 21*). Thawed aliquots of the SeMet GlpOΔ protein were buffer-exchanged into 1 mM sodium *N*-(2-hydroxyethyl)piperazine-*N*′-2-ethanesulfonic acid (pH 7.2) to give a final protein concentration of 10 mg/mL. Crystals were grown in 24-well sitting-drop plates over reservoirs of 0.5 mL, using drop sizes of 4 + 4 μL. Large single crystals of SeMet GlpOΔ grew best using a reservoir solution of 0.2 M Na_2SO_4, 17−22% PEG3350, and 10 mM β-mercaptoethanol, with glycerol (20−35%) present as the cryoprotectant. Crystals appeared within 1 day, growing to full size in 2−3 days, and were flash-frozen in a nitrogen stream at 100 K directly after being removed from the drop. Data sets for MAD phasing were collected at National Synchrotron Light Source beamline X26C. Although we have no evidence that any flavin reduction occurred during synchrotron data collection with either intact GlpO or GlpOΔ crystals, we cannot eliminate

Table 1: Data Collection for GlpO and GlpOΔ and Phasing Statistics for GlpOΔ

		GlpOΔ[b]		
	GlpO[a]	edge	peak	remote
wavelength (Å)	0.9296	0.9790	0.9783	0.960
space group	$P2_1$[c]		$P2_12_12$	
cell dimensions				
a, *b*, *c* (Å)	128.36, 106.78, 58.89		86.21, 95.48, 77.61	
α, *β*, *γ* (deg)	90, 99.18, 90		90, 90, 90	
resolution (Å)	2.40	2.10	2.10	2.10
no. of reflections	141187	248145	238765	233374
no. of unique reflections	57965	37395	36799	37759
completeness (%)	94.8 (97.4)[d]	97.7 (83.7)	96.5 (85.4)	98.7 (89.6)
R_{sym} (%)	6.4 (29.8)[e]		7.4 (32.4)	
I/σ	9.9 (2.8)		12.9 (4.0)	
phasing power[f]		0.9	1.26	
resolution range (Å)		41.78−2.10	41.76−2.10	41.79−2.10
figure of merit[g]		0.60		

[a] Collected with crystals of native intact GlpO at the Cornell High-Energy Synchrotron Source F-1 station using an ADSC Quantum-4 CCD detector (*21*). [b] Collected with crystals of SeMet GlpOΔ at beamline X26C of the National Synchrotron Light Source using an ADSC Quantum-4 CCD detector. [c] The space group assignment given in ref *21* is incorrect; the correct space group is $P2_1$. [d] Numbers in parentheses represent data for the highest-resolution shell. [e] R_{meas} for native intact GlpO as taken from ref *21*. [f] Calculated to 2.9 Å resolution. [g] Computed after solvent flattening using RESOLVE.

this possibility. Crystals of native GlpOΔ were obtained under very similar conditions, omitting glycerol and *β*-mercaptoethanol; cryoprotectant soaks using a solution of 0.3 M Na_2SO_4, 25% PEG3350, and 15% glycerol were optimized for these GlpOΔ crystals.

GlpOΔ Phasing and Structure Refinement. Images in each MAD data set were indexed, integrated, and scaled in d*TREK (*24*); data collection and phasing statistics are summarized in Table 1. SOLVE (*25*) was used to locate all 12 of the Se sites; density modification was performed with RESOLVE (*26*, *27*). The resulting electron density map led to an initial model which was subjected to refinement with REFMAC5 (*28*). Water molecules, identified with COOT (*29*) in the $F_o - F_c$ map using a 3σ difference Fourier cutoff, were visually confirmed and added at this stage. Also, one clear sulfate ion was added to the model. As refinement progressed, the electron density indicated that a bent conformation for the flavin isoalloxazine, along the FAD−N5−N10 axis, was required. The butterfly conformation was added and refined in CNS (*30*); final refinement of the full model was also performed with CNS, and refinement statistics for the GlpOΔ structure are summarized in Table 2.

Intact GlpO Structure Solution and Refinement. Since the intact GlpO differs from GlpOΔ only by the absence of the His-tag and the presence of Asp356−Ala405 (essentially, the 50-residue insert sequence), the GlpOΔ coordinates (minus the FAD, sulfate ion, and solvent waters) were used as the search model for the intact GlpO molecular replacement solution [using PHASER (*31*, *32*)] to locate two molecules in the asymmetric unit, using data from 30 to 2.50 Å resolution. Phasing and density modification were also performed with PHASER. Early rounds of refinement extending out to the limit of resolution (2.4 Å) were performed with CNS, with solvent waters being added as for GlpOΔ. In accordance with the electron density appearance, a butterfly flavin conformation was added for chain A, but the chain B flavin was left planar. The latter stages of refinement were carried out with REFMAC5.

Table 2: Crystallographic Refinement Statistics for GlpO and GlpOΔ

	GlpO[a]	GlpOΔ
resolution range (Å)	12.0−2.40	41.76−2.30
amplitude cutoff	none	none
no. of amino acid residues	1087	546
no. of waters	232	271
no. of sulfate ions		1
no. of total non-hydrogen atoms	8870	4618
R_{factor} (%)	23.8	21.0
R_{free} (%)	24.6	25.3
stereochemical ideality		
bond length rmsd (Å)	0.012	0.015
bond angle rmsd (deg)	1.7	1.3
φ and *ψ* most favored (%)	85.0	89.1
φ and *ψ* additional allowed (%)	14.6	10.5
φ and *ψ* generously allowed (%)	0.3	0.4

[a] Intact GlpO dimer.

RESULTS AND DISCUSSION

Kinetic and Redox Properties of GlpOΔ. The GlpOΔ deletion mutant, lacking residues Asp356−Ala405, was designed to test the role of the ca. 50-residue insert that is present in GlpO but not GlpD enzymes (*9*). GlpOΔ differs from nicked GlpO (*20*) in that the limited proteolysis cleavage sites correspond to Lys368 and Lys404; nicked GlpO therefore includes 14 additional residues (Asp356−Lys368 and Ala405) not present in GlpOΔ. In dithionite and sulfite titrations (Figure 1), GlpOΔ behaves like both intact and nicked enzymes (*20*). The tightly bound flavin is reduced directly on titration with 1.1 equiv of dithionite, and there is no evidence for any stable semiquinone intermediate. Sulfite titration of GlpOΔ gives the stable flavin N5−sulfite adduct, with a K_d of 0.92 mM at pH 7.0 and 25 °C. Enzyme-monitored turnover analyses with GlpOΔ (Figure 2) [10 *μ*M enzyme and 0.77 mM O_2 over the Glp concentration range of 2.5−50 mM (pH 7.0, 5 °C)] demonstrate that His-tagged GlpOΔ is catalytically active, with a k_{cat} of 11.2 ± 0.5 s^{-1} and a K_m(Glp) of 6.6 ± 1.0 mM (Table 3). Interestingly, whereas the k_{cat} is similar to that of nicked GlpO, the K_m(Glp) is 5.5-fold lower, leading to a 4.4-fold increase in

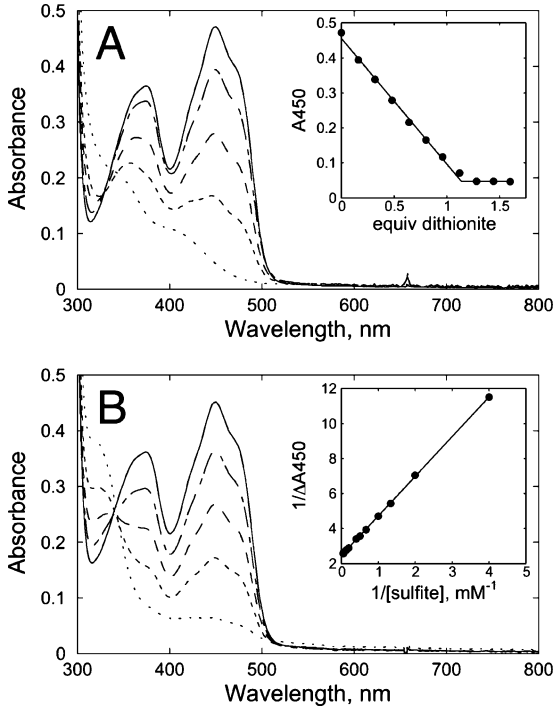

FIGURE 1: Dithionite and sulfite titrations of GlpOΔ. (A) The enzyme [40.8 μM, in 0.8 mL of 50 mM potassium phosphate (pH 7.0) and 0.5 mM EDTA] was titrated with a 3.9 mM solution of dithionite. Spectra shown, in order of decreasing absorbance at 450 nm, correspond to the addition of 0 (—), 0.16 (—•—), 0.48 (— — —), 0.8 (- - -), and 1.28 equiv (•••) of dithionite/FAD. The inset shows the absorbance change at 450 nm vs the amount of added dithionite. The end point corresponds to 1.14 equiv of dithionite/FAD. (B) The enzyme (39.1 μM, prepared as above) was titrated with sodium sulfite solutions of 0.1 and 1.0 M. Spectra shown, in order of decreasing absorbance at 450 nm, correspond to the addition of 0 (—), 0.25 (—•—), 0.75 (— — —), 2 (- - -), and 17.5 mM (•••) total sulfite ($HSO_3^- + SO_3^{2-}$). The inset shows a double-reciprocal plot of the absorbance change at 450 nm vs added sulfite concentration.

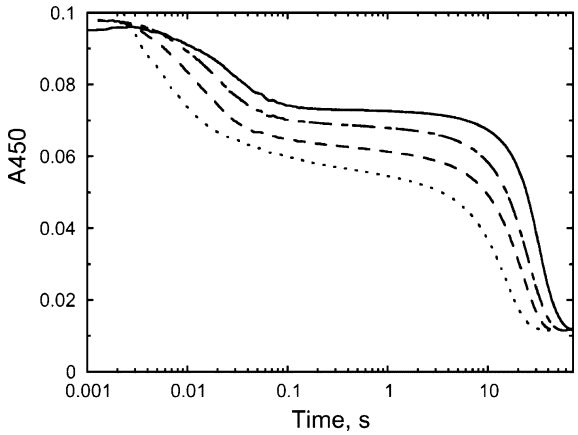

FIGURE 2: Enzyme-monitored turnover of GlpOΔ. The enzyme [9.9 μM after mixing, in air-equilibrated 0.1 M phosphate (pH 7.0) and 0.5 mM EDTA] was mixed at 5 °C with different concentrations of Glp [2.5 (—), 5 (—•—), 10 (— — —), and 50 mM (- - -)] that had been equilibrated with 100% O_2 in the same buffer. The reactions were followed at 450 nm.

the GlpOΔ specificity constant (Table 3). The higher K_m(Glp) of nicked GlpO compared with that of GlpOΔ, even though nicked GlpO retains more residues, is surprising and suggests that the 14 additional residues in nicked GlpO do not contribute substantially to catalysis but actually appear to somehow interfere with Glp binding and/or catalysis. One possible interpretation, for example, would invoke the larger E* component (*9*, *20*) in the resting nicked enzyme population.

Table 3: Steady-State Kinetic Constants for Intact and Nicked Forms of *Streptococcus* sp. GlpO and for GlpOΔ

	intact[a]	nicked[a]	GlpOΔ[b]
K_m(Glp) (mM)	1.9	36.2	6.6
$K_m(O_2)$ (μM)	52	69	460
k_{cat} (s^{-1})	17.9	14.1	11.2
k_{cat}/K_m(Glp) (M^{-1} s^{-1})	9.4×10^3	390	1.7×10^3

[a] From ref *20*. [b] Calculated from the data in Figure 2.

Structure Solutions of GlpOΔ and Intact GlpO. Given the absence of suitable search models for a molecular replacement solution with the 2.4 Å data set collected with the native *Streptococcus* sp. GlpO (*21*), we prepared the SeMet derivatives of N-terminal His-tagged and wild-type (non-His-tagged) intact GlpO, but neither of these allowed us to reproduce the previously reported (*21*) crystal form. However, with the SeMet derivative of His-tagged GlpOΔ, novel well-diffracting crystals were grown, and a three-wavelength MAD data set was collected to determine the structure (Table 1). The crystals have a single molecule in the asymmetric unit, and the final GlpOΔ model (refined using data to 2.30 Å resolution) comprises residues 0−350 (one residue from the His-tag precedes the wild-type initiating Met) and residues 412−606, the FAD cofactor, and ordered solvent; it has an R_{factor} of 21% (R_{free} = 25.3%) with good geometry (Table 2). Missing from the model and presumed mobile are the first 13 residues of the N-terminal His tag, residues 351−355 and 406−411 bordering the two ends of the deletion, and the C-terminal residue Lys607.

The crystal structure of intact GlpO, determined by molecular replacement using GlpOΔ, has two chains in the asymmetric unit. Refinement at 2.4 Å resolution led to a final model with reasonable statistics (Table 2). Due to lack of electron density, chain A is missing residues 361−407, residue 518, and C-terminal residues 606−607; chain B, apparently less well-tethered, is missing electron density for residues 16, 17, 111, 112, 203, 245, 246, 361−408, 476−494, and 516−518. The common major disordered segment (residues ~361−407) corresponds well with the region deleted in GlpOΔ. All seven short segments missing in chain B are involved in crystal contacts in chain A, explaining their better definition. The two subunits have an overall C_α rmsd of just 0.5 Å; this agrees well with the expected coordinate errors (*33*) of 0.33 and 0.38 Å for the well-ordered parts of the GlpOΔ and intact GlpO models, respectively. Detailed descriptions of the intact structure will focus on chain A, with residues from chain B being designated by a prime symbol (e.g., His65, chain A; His65′, chain B). The $2F_o - F_c$ maps for the respective FAD coenzymes illustrate the quality of electron density for well-ordered regions of both structures (Figure 3).

Overall Structure. Comparison of the molecular packing in the GlpO and GlpOΔ crystal forms reveals one common packing interaction that buries the most surface, and we interpret this to represent the physiologically relevant dimer (Figure 4A); both refined structures show the same overall chain fold (Figure 4B). Each chain (taking the GlpOΔ

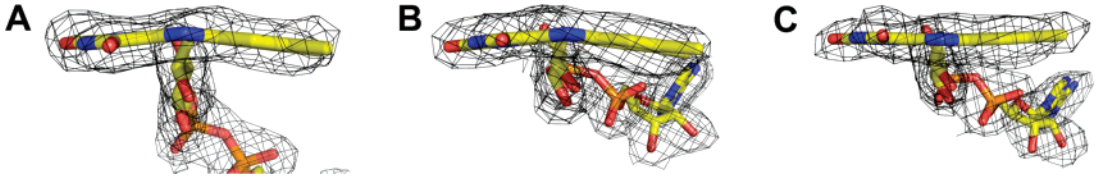

FIGURE 3: Final $2F_o - F_c$ maps for the FAD redox centers of GlpOΔ (A), intact GlpO chain A (B), and intact GlpO chain B (C), together with the refined models. Carbon atoms are colored yellow; others are color-coded by atom type. A portion of the FAD in panel A has been omitted for clarity. The depicted contour level is 1σ.

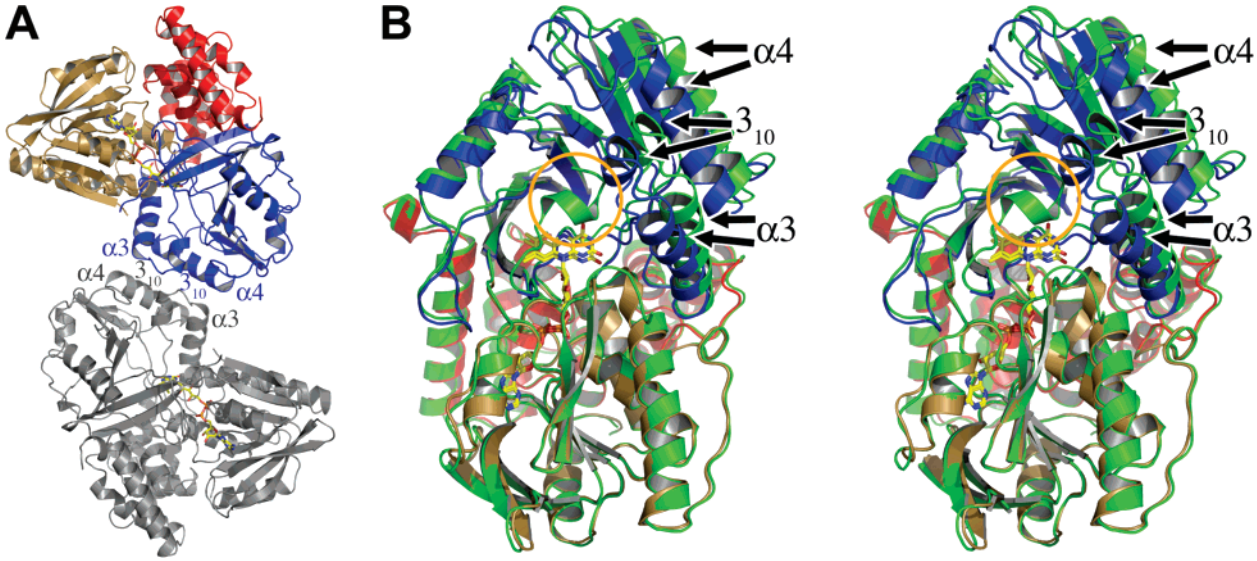

FIGURE 4: GlpOΔ dimer and superposition of a GlpOΔ monomer with intact GlpO chain A. (A) One subunit (top) of the GlpOΔ dimer is color-coded by domain: sand for the FAD-binding domain, blue for the dimerization/substrate-binding domain, and red for the C-terminal domain. Both FADs are color-coded as in Figure 3, and helical elements providing the main interactions in the dimer interface are labeled. (B) Superposition, in stereo, based on the FAD-binding domain gives a rmsd of 1.1 Å for a GlpOΔ monomer (color-coded as in panel A) and intact GlpO chain A (green). Both FADs are color-coded as in panel A. An ~3 Å shift in a portion of domain 2 (helical elements indicated by arrows) accompanies insertion of the additional loop and short helix (circled) near the flavin of intact GlpO.

structure as the point of reference) is organized as three compact domains [Figure 5A, as assigned with DSSP (*34*)]: domain 1, a FAD-binding domain that consists of three chain segments (residues 1−58, 173−254, and 412−452) and has a central six-stranded β-sheet; domain 2, a dimerization and putative substrate-binding domain that consists of two chain segments (residues 59−172 and 255−350) and has a mixed, eight-stranded β-sheet; and domain 3, a C-terminal domain that is a single-chain segment (residues 453−606) and is largely α-helical. The proteolytically labile ~50-residue insert unique to GlpO enzymes (*9*) and deleted in GlpOΔ is, as expected, not present as an integral part of the structure but is a largely disordered segment that bridges the second segment of domain 2 and the third segment of domain 1 (Figure 5A). The distance ($C_\alpha - C_\alpha$) between residues 349 and 413 that must be bridged by the segment is only 7.4 Å. This short distance leads us to suspect that the insert may be a segment that is a small folded domain on its own but has few interactions with the rest of the protein and thus is not fixed in the crystal structure. In terms of the overall structure, there are two related differences between intact GlpO and GlpOΔ. The first is that GlpO has additional ordered residues (356−360) corresponding to positions 2−6 of the 50-residue insert, and these residues (plus residues 351−355) form a loop and short helix that sits just above the flavin in the cleft between domains 1 and 2 (Figure 4B) and represents one significant difference. Associated with the insertion of these 10 residues into the cleft is the shift by ~3 Å of a portion of domain 2 that includes helices 3 and 4. As discussed in detail in a later section, we interpret the more "open" GlpOΔ conformation as being equivalent to the fully active resting oxidized enzyme (E) form; we interpret the more "closed" intact GlpO structure as being representative of the E* form.

In a search for structurally similar proteins (*35*), the top four scores correspond to *B. subtilis* glycine oxidase [ThiO; rmsd = 3.0 Å, 19% identity, $Z = 28.2$ (*36*)], the *Pyrococcus horikoshii* L-proline dehydrogenase β-subunit [rmsd = 3.1 Å, 19% identity, $Z = 27.9$ (*37*)], the β-subunit of *Pseudomonas maltophilia* heterotetrameric sarcosine oxidase [rmsd = 3.3 Å, 14% identity, $Z = 25.3$ (*38*)], and *Bacillus* sp. monomeric sarcosine oxidase [MSOX; rmsd = 3.4 Å, 14% identity, $Z = 24.1$ (*39*)]. Pig kidney D-amino acid oxidase [DAAO (*40*)] yields a rmsd of 3.3 Å and 16% identity ($Z = 22.7$). All five of these proteins belong to the GR_2 subfamily of FAD-dependent enzymes (*41*) and consist of two domains (FAD-binding and substrate-binding, or interface) that are similar to the first two domains of GlpO. In terms of backbone rmsd and catalytic mechanism, ThiO (*36*) appears to be the structurally known homologue most similar to GlpO and will be used for most comparisons below.

A topology diagram of the first two domains of GlpO (Figure 5A) reveals a fold that is remarkably similar to that of ThiO, in fact conserving every element of secondary structure (see Figure 5 of ref *36*). The spatial arrangement of the two domains is also quite similar (Figure 5B),

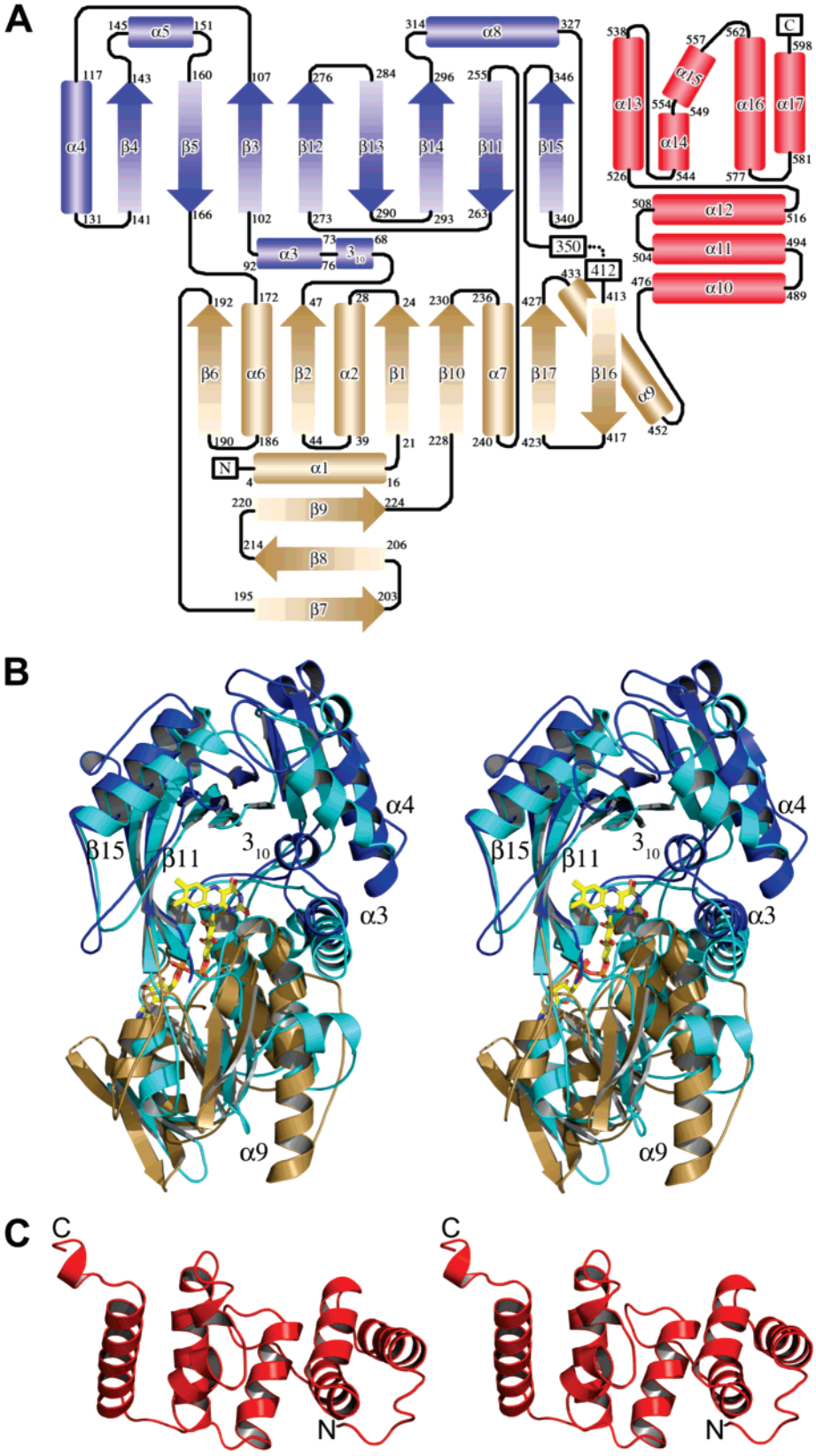

FIGURE 5: Topology diagram for GlpOΔ and superposition of GlpOΔ domains 1 and 2 with a ThiO monomer. (A) Each secondary structural element, as assigned by DSSP (*34*), is color-coded by domain, as in Figure 4, and the respective first and last residue numbers are labeled. The single 3_{10}-helix shown corresponds to that in Figure 4. The location of the 50-residue insert, deleted in GlpOΔ and largely disordered in the intact GlpO structure, is also indicated (⋯). (B) Superposition, in stereo, of GlpOΔ domains 1 and 2 (color-coded as in Figure 4) and a ThiO monomer (cyan). DALILITE gives a rmsd of 3.0 Å for 330 C_α atoms with 19% sequence identity ($Z = 28.2$). Both FADs are color-coded as in Figure 3; secondary structural elements described in the text (with the exception of α1) are labeled. (C) Stereoview of the GlpOΔ C-terminal domain. The orientation, relative to that of domains 1 and 2 in panel B, is given in Figure 4B. C_α positions corresponding to the N- and C-termini (Gly468 and Glu606, respectively) are labeled. This domain, which consists of eight α-helices organized into two bundles, is absent in ThiO and other DAO pfam members.

suggesting that there is little new to describe about these two domains, compared with ThiO. The one new and unique feature is the dimerization interface of GlpO. Although ThiO and DAAO both have quaternary structure, neither has the same interface as GlpO. The GlpO dimer interface is rather small, burying a total surface area of 640 Å^2 per monomer (~3% of each monomer surface), with residues from the substrate-binding domain providing the bulk of the contact area. The main interactions involve residues from helix α4 and the loop connecting helices 3_{10} and α3, which pack across the 2-fold symmetry axis with the same structural elements of the other chain (Figure 4A).

In contrast to the first two domains, the structural similarity search also shows that the GlpOΔ C-terminal domain (Gly453−Glu606) is a novel fold. This domain is an aggregation of eight α-helices (Figure 5C) which are organized into a three-helix bundle (α10−α11−α12) followed by a four-helix bundle (α13−α14/α15−α16−α17), where the two short bent helices 14 and 15 take the place of one longer helix. Both helical bundles have simple "up−down−up" topology; when viewed down α1 (from the N-terminus), helices α17−α16−α13−α12−α10 form a surface-exposed helical skirt that covers the back of the FAD-binding domain. Although the functional importance of this domain is unknown (see below), it appears to be conserved in all known GlpO and GlpD sequences (Figure 6).

FAD−Protein Interactions. During refinement of the GlpOΔ structure, we noticed that the FAD isoalloxazines in both GlpOΔ and in intact GlpO chain A appear to be bent along the N5−N10 axis, with angles of ~12° (Figure 3). In contrast, the electron density for the GlpO chain B flavin, which has *B*-factors similar to those for the chain A flavin, could be fit well with a planar flavin (Figure 3). At the 2.4 Å resolution of this analysis, we cannot conclude that the chain B flavin is perfectly planar, but we do conclude that the chain B flavin is much less bent than the others. Interestingly, neither ThiO, MSOX, nor DAAO shows bent flavins, so this appears to be an unusual feature of GlpO.

While similar bent butterfly flavin conformations are characteristic of reduced flavins and flavoproteins [e.g., reduced thioredoxin reductase (*42*) and the reduced PutA proline dehydrogenase domain (*43*)], there are fewer examples for oxidized flavoenzymes. Lennon et al. (*42*) identified three cases in which the oxidized isoalloxazine bending angle is greater than 18°: pyruvate oxidase (PDB entry 1POW), NADH oxidase (PDB entry 1NOX), and trimethylamine dehydrogenase (PDB entry 2TMD). Most recently, Schiffer et al. (*44*) have identified a butterfly conformation for the oxidized FAD in adenosine-5′-phosphosulfate reductase; as with trimethylamine dehydrogenase, this has also been considered as an energetically favorable factor in catalysis. The bent oxidized flavin in GlpO may have a similar redox impact, as the FAD/$FADH_2$ redox potential for the *En. casseliflavus* enzyme has been measured to be −118 mV (*9*), roughly 100 mV higher than that for free FAD (−219 mV). Since the redox potential for the Glp/DHAP couple is −190 mV (*45*), the effect of the GlpO apoprotein in providing a thermodynamically favorable system for Glp dehydrogenation includes an environment that favors the FAD-N1/O2α-anionic form of $FADH_2$ as well as the butterfly conformation of oxidized FAD. Also, as studies of ThiO, MSOX, and DAAO indicate that the substrate binds at the flavin *re* face (*36*, *39*, *40*), this "butterfly" bending of the flavin pyrimidine and dimethylbenzene rings away from the *re* face would direct FAD-N5 toward the Glp substrate and promote reactivity (see below).

The hydrogen bonding interactions of GlpOΔ with FAD are rather similar to those seen for other GR_2 subfamily flavoenzymes (*41*). The ADP portion of the FAD interacts, as for the classic nucleotide-binding fold (*46*), mostly via residues from the first βαβ portion of the fold, including the pyrophosphate-interacting GxGxxG fingerprint (here GGGITG) and a carboxylic acid side chain (here Glu48) at the end of the second β-strand (*47*). The adenine is bound in a pocket surrounded by Ile24, Met49, Ser232, Trp235, and Val239. All of the interactions shown with the ADP portion of FAD are also seen in both chains A and B of intact GlpO, and the side chains involved are well-conserved in the bacterial GlpOs and GlpDs given in Figure 6.

In terms of interactions with the flavin itself, in GlpOΔ the main chain Ile430-N and Thr431-N hydrogen-bond with FAD-O2α as does Thr431-OG, consistent with the expectation of the stabilization of a negative charge at this locus (*8*, *9*). Lys429-NZ sits just 3.5 Å above the FAD-C2 atom, so its positive charge will further stabilize anionic FAD N1/O2α forms. The FAD-N3 pK_a for intact *En. casseliflavus* GlpO is decreased to 8.5 (from 10.4 for free FAD), entirely consistent with these observations (*8*). We have reported (*20*) that this pK_a value appears to be further decreased for intact *Streptococcus* sp. GlpO, since very little visible absorbance change was observed during a spectral pH titration of the latter enzyme between pH 8.5 and 10. There is no significant change in this active-site pK_a with the nicked *Streptococcus* sp. GlpO, and we similarly expect no significant change for GlpOΔ. Other notable interactions with the flavin include hydrogen bonds with FAD-N5 by Thr61-OG (which in turn receives a hydrogen bond from His259-NE2) and with FAD-N3 by Leu63-O. In terms of nonpolar packing interactions, Ile430 (from the loop preceding helix α9) packs against the pyrimidine ring, while Gly257, Gly344, and Leu345 (from strands β11 and β15) have similar interactions with the dimethylbenzene ring, showing that residues from domain 2 block solvent access in this region. The MSOX equivalent of β15 carries the Cys315 covalent attachment (through FAD-C8α) site (*39*). As we will discuss later in the context of substrate binding, the side chains of Ser60, His65, Arg69, Tyr70, His259, Thr298, Arg346, and Lys429 line the pocket just above the *re* face of the flavin. Also in this region are three backbone amides: Gly67-N forms a hydrogen bond with His65-ND1, and both Ile68-N and Arg69-N hydrogen bond with waters. Interestingly, interactions between Ser60 and Lys62-N stabilize a backbone conformation that allows Thr61-N to point directly at FAD-C4a. ThiO (Ala47-N and Gly48-N) and pig kidney DAAO (Trp52-N) have similar interactions with the respective FAD-C4a; the high-resolution crystal structure of the yeast DAAO complex with D-Ala (*48*) has provided evidence for a covalent hydroperoxide, most likely bonded via FAD-C4a.

In intact GlpO (both chains A and B), the flavin environment is rather different because the insertion of residues 351−360 into the active-site pocket is associated with a shift in the flavin and the reorganization of surrounding residues (Figures 4B and 7). The bent oxidized flavins (intact chain A and GlpOΔ) superimpose well in the vicinity of FAD-

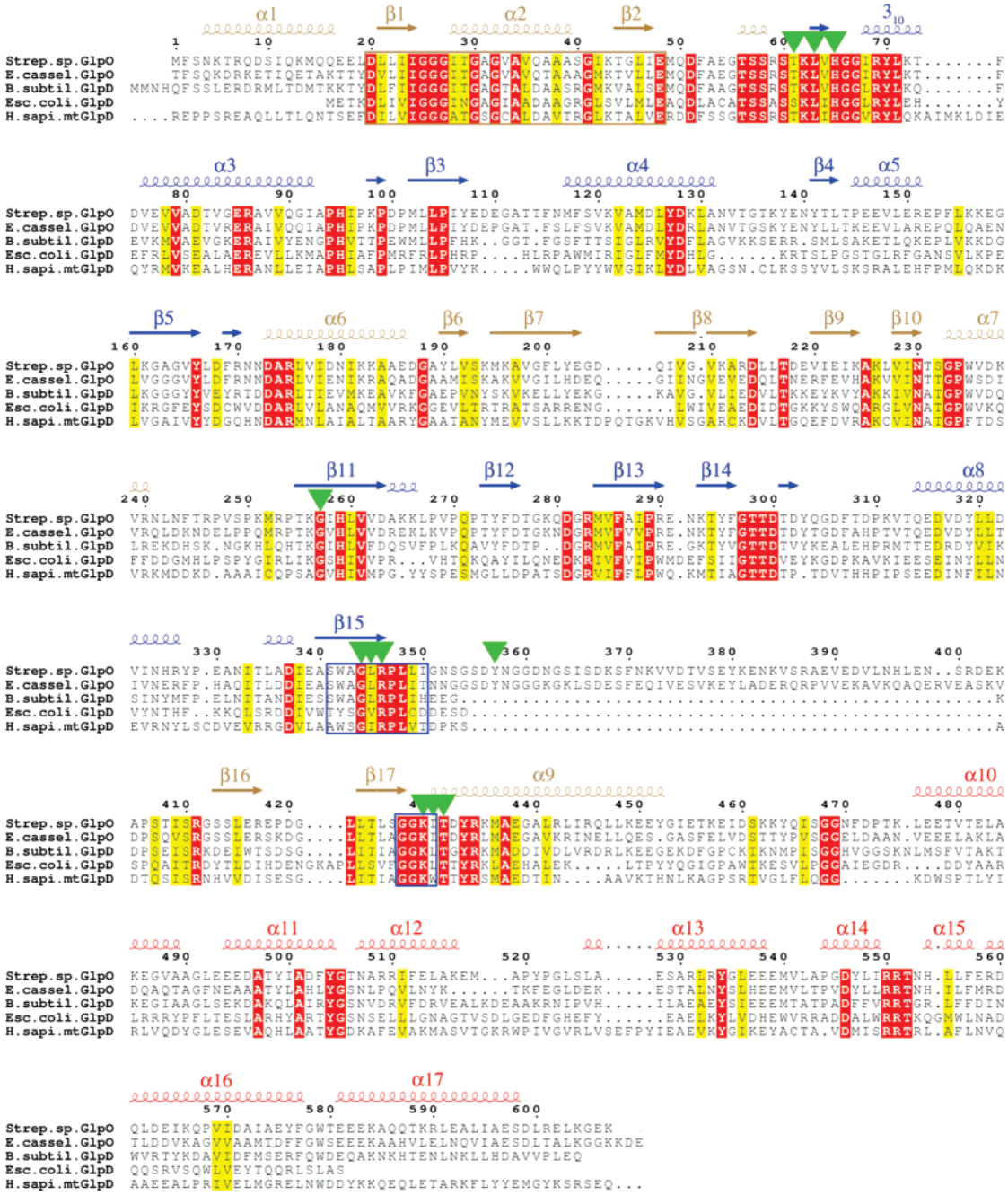

FIGURE 6: Structure-based sequence alignment for *Streptococcus* sp. GlpO and four known functional GlpOs and GlpDs from bacterial and mitochondrial sources (references given in the text). The residue numbering corresponds to both intact and deletion mutant forms of *Streptococcus* sp. GlpO, where GlpOΔ lacks residues 356−405. Residues 1−51 and 690−805 of the human mitochondrial GlpD (*H.sapi.mt*; full-length precursor sequence) have been omitted for clarity. Red and yellow blocks are conserved residues and conservative substitutions, respectively. Boxes represent FAD-binding (sand) and putative Glp-binding (blue) segments, as defined previously (*20*). Secondary structure assignments (color-coded by domain) correspond to GlpOΔ. Green triangles denote those active-site residues shown in Figure 7 and residues involved in both hydrogen bonding and hydrophobic interactions with the FAD isoalloxazine in GlpOΔ. The position of Tyr357 in the intact enzyme structure suggests that this active-site conformation represents the E* state.

C8, and they diverge to give separations of 2−3 Å of the pyrazine and pyrimidine moieties. This shift contributes to the different protein interactions with the latter, with the Ile430-N, Thr431-N, and Thr431-OG interactions in GlpOΔ being replaced by a Lys429-NZ−FAD-O2α interaction in intact GlpO. Also, the Leu63-O−FAD-N3 hydrogen bond is not seen in the intact enzyme. Tyr357 of GlpO stacks neatly above the *re* face of the central pyrazine ring, with a Tyr357-CE1−FAD-N10 distance of 3.4 Å. Tyr357 comes at the N-terminus of the 50-residue insert (*20*), is present in nicked GlpO, and is deleted in GlpOΔ. Intact GlpO chain A also reveals direct solvent water interactions with both FAD-O4α and -N5; the latter interaction replaces that observed between Thr61-OG and FAD-N5 in GlpOΔ. Similarly, GlpOΔ lacks this direct solvent water interaction.

Glp Binding and the Active Site. Austin and Larson (*5*) were the first to deduce sequence motifs for the "Glp-binding domain" in *E. coli* GlpD. These were based on limited sequence similarity between GlpD and *E. coli* triosephosphate isomerase, focused on the residues of the latter enzyme that interact with the phosphate of the bound DHAP substrate (*49*) [and with Glp (*50*)]. Interestingly, two of these

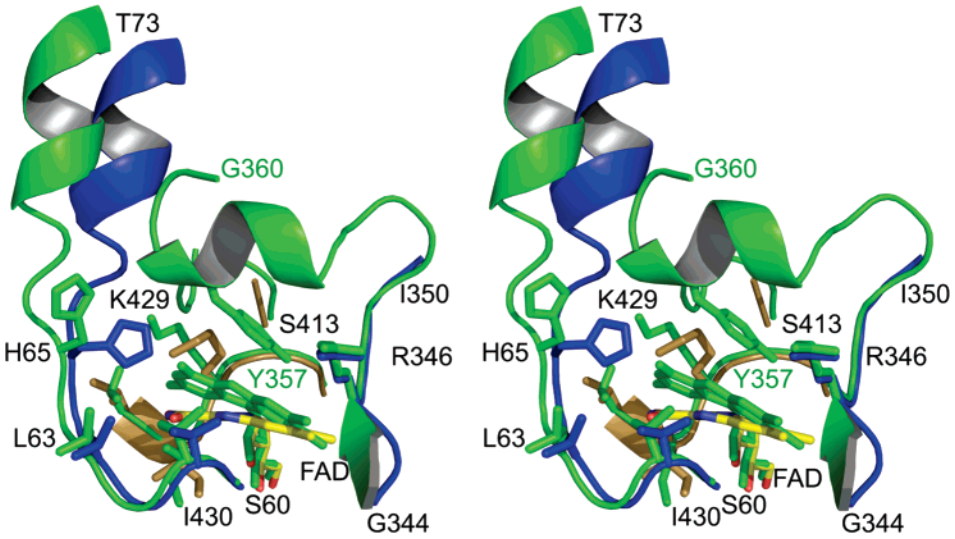

FIGURE 7: Active-site overlay, in stereo, of GlpOΔ and intact GlpO. The superposition was performed as described in the legend of Figure 4B. Intact GlpO protein and FAD are colored green (residues 351−360, including the short helical insert, are unique to the intact GlpO structure). GlpOΔ is color-coded by domain, as in Figure 4; the GlpOΔ FAD is color-coded by atom type. In this view, the 3_{10}-helices of both proteins (as shown in Figure 4B) are also depicted.

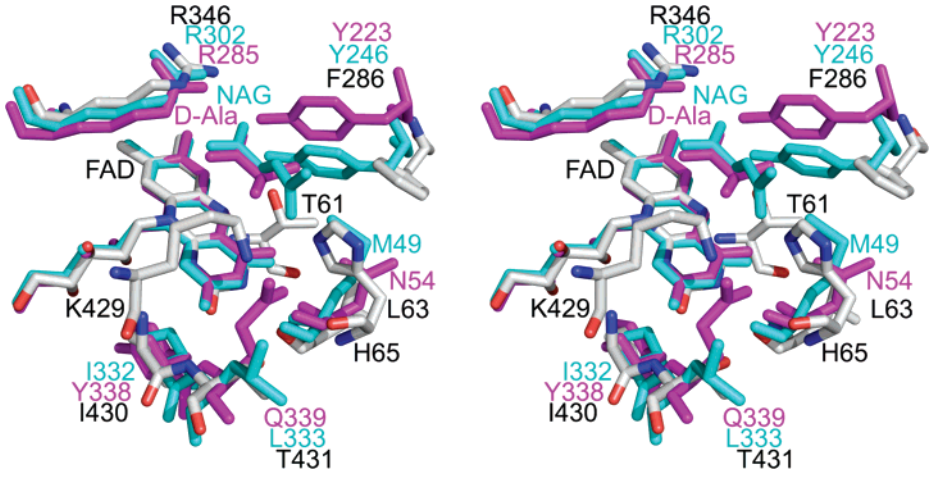

FIGURE 8: Active-site overlay, in stereo, for GlpOΔ, the ThiO−*N*-acetylglycine (NAG) complex (chain A), and the yeast DAAO−D-Ala complex. The superposition was performed on the basis of the AMP moieties of the respective FAD. GlpOΔ side chains and FAD are color-coded by atom type, the ThiO−NAG complex is colored cyan, and the DAAO−D-Ala complex is colored magenta. GlpOΔ His65 and Lys429 have no structural equivalents in either ThiO or DAAO.

sequence motifs, Ser341−Ile350 and Gly427−Ile430, closely flank the 50-residue insert in GlpO. The GlpOΔ structure also shows that residues from these segments [Gly344, Leu345, Arg346, and Ile430 (and Thr431)] actually are part of the active site, interacting with or lining the pocket above the flavin.

Attempts to soak Glp into GlpOΔ crystals have led to cracked crystals that do not diffract, implying that some conformational change occurs during Glp binding and/or turnover. In the absence of a ligand-bound structure, and to gain insight into the substrate binding mode and catalytic mechanism, we carried out overlays of GlpOΔ (representing the open conformation of GlpO) with the ThiO−*N*-acetylglycine and yeast DAAO−D-Ala complexes. As seen in Figure 8, GlpOΔ Arg346, conserved in the GlpO and GlpD sequences, is remarkably structurally similar with the key residues ThiO Arg302 (*36*) and yeast DAAO Arg285 (*48*), providing a direct link to these active sites. Further active-site similarities include the main chain hydrogen bonding interactions with the respective FAD-O2α (equivalent to Ile430 and Thr431 of GlpOΔ) and FAD-N3 (equivalent to Leu63 of GlpOΔ). A difference is that a Tyr residue interacting with the substrate carboxylate in yeast DAAO (Tyr223), which is structurally similar to Tyr246 of ThiO, is replaced by Phe286 in GlpOΔ, leaving more space in this region. At the other end of the substrate-binding pocket, GlpOΔ residues His65, Arg69, Tyr70, and Lys429 have no equivalents in ThiO or DAAO but offer positively charged/hydrogen bonding side chains, well-positioned to interact with substrate and conserved in GlpO and GlpD sequences. Accordingly, on the basis of the open GlpOΔ structure, we propose the following Glp recognition and dehydrogenation scheme (Figure 9). As the Glp substrate approaches the flavin *re* face, the Glp phosphate is attracted to the pocket surrounded by Lys429, His65, Arg69, and Tyr70 with Glp C1-OH anchored by interaction with Arg346. Early work with crude preparations of the *mito*GlpD from insect flight muscle (*51*) showed that substitution of Glp C1-OH with either H (1-deoxy-Glp) or F (1-deoxy-1-fluoro-Glp) led to a 60−80-fold decrease in k_{cat}/K_m for the respective

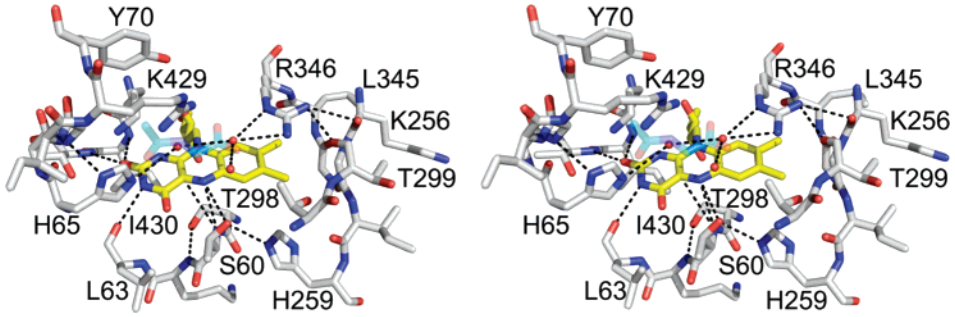

FIGURE 9: Stereoview of the proposed Glp-binding pocket, including *N*-acetylglycine (NAG) from the ThiO overlay in Figure 8. GlpOΔ residues and FAD (yellow carbon atoms) are color-coded by atom type; NAG (cyan carbon atoms) is rendered as a 50% transparency. Three active-site water molecules are colored red; hydrogen bonding interactions and a well-aligned close approach (3.8 Å) of Thr61-N to FAD-C4a are described in the text. The respective first and last residues of each peptide segment are labeled, with the exception of Gly344.

substrate, demonstrating that Glp C1-OH is indeed an important determinant for substrate recognition and catalysis.

The oxidation of the secondary alcohol function in Glp can be compared with the mechanisms for amino acid oxidation as catalyzed by other members of the DAO pfam (*52*), such as ThiO, MSOX, and DAAO. For yeast DAAO, the structure of the complex with D-Ala at 1.20 Å resolution (*48*) clearly shows the substrate C_α-H pointing toward FAD-N5, entirely consistent with the hydride transfer mechanism proposed by Mattevi et al. (*40*). There is no acid−base catalyst; the rate of D-Ala oxidation is 7 orders of magnitude greater than that for D-lactate, reflecting the relative pK_a values of α-NH_3^+ versus α-OH. A very similar mechanism has been suggested for ThiO (*36*), as the structure of the *N*-acetylglycine complex positions C_α-H almost directly above FAD-N5 at a distance of 3.5 Å. No acid−base catalyst is present, and in both DAAO and ThiO, the anionic reduced FAD is stabilized by protein interactions with the N1/O2α locus. While earlier evidence implicated His269 (*39*, *53*) and/or Tyr317 (*54*) as potential acid−base catalysts in the MSOX−substrate complex, more recent mutagenesis studies have demonstrated that ionization of the complex, as required for enzyme reduction, is independent of either residue. A hydride transfer mechanism has been considered for MSOX and would seem to be preferred in light of these mutagenesis studies (*54*). While the hydride transfer mechanism preferred for GlpO (*8*, *9*, *20*) resembles those discussed above, the GlpO mechanism is unique in requiring ionization of the Glp C2-*OH*. Recent structure-based mechanisms for the NAD^+-linked (flavin-independent) Glp dehydrogenases from *Leishmania mexicana* (*55*) and from human liver (*56*) both implicate a Lys residue in ionization of Glp C2-OH, thus promoting transfer of a hydride to the NAD^+ acceptor. With respect to the identity of the proposed active-site base in GlpO, His65 is reasonably well-positioned to interact with and abstract the Glp C2-OH proton, but the hydrogen bonding Gly67-N−His65-ND1 hydrogen bonding interaction observed in the GlpOΔ structure implies that His65 is monoprotonated on NE2. In this sense, His65 could not serve as an acid−base catalyst, unless a conformational change disrupts that interaction.

GlpOΔ as a Structural Template for the GlpDs. Sequence alignments for GlpOΔ with the GlpDs from *E. coli* (*5*) and human mitochondria (*57*) give levels of identity of ∼30% over the entire GlpOΔ sequence; with *B. subtilis* GlpD (*6*), the level of identity is 45%. Now, with the GlpOΔ structure in hand, we can assess the level of active-site conservation and evaluate proposals for how *mito*GlpD, in particular, is anchored to the membrane. As seen in Figure 6, the FAD-binding motif and nearly all of the key active-site residues described above are conserved. The structure also reveals that the 50-residue insert unique to the GlpOs (and deleted in GlpOΔ) does not contribute in a major way to the active site, and the chains at the two ends of the deleted region are just 7.4 Å apart, close enough to be bridged by the three or four residues in GlpD (*B. subtilis* residues 357−360) without altering the chain path.

The structure now also reveals clearly that there are no portions of the GlpD sequence that could serve as transmembrane helices, as all parts (except for the mammalian *mito*GlpD calmodulin homology domain) are incorporated into the three domains seen in the GlpO structure. In this light, we have reevaluated the predicted membrane topology of the human mitochondrial, *E. coli*, and *B. subtilis* GlpDs with five contemporary transmembrane helix prediction protocols: PHOBIUS (*58*), THUMBUP (*59*), TUPS (*59*), the SPLIT 4.0 SERVER (*60*), and UMDHMM^{TMHP} (*59*). Apart from the N-terminal mitochondrial signal peptide predicted by PHOBIUS and the SPLIT 4.0 SERVER [Brown et al. (*3*) reported that the rat *mito*GlpD precursor is cleaved following Ala42], the consensus prediction by all five algorithms is that there are no transmembrane helices. For the human *mito*GlpD sequence, UMDHMM^{TMHP} and PHOBIUS identify two possible weak transmembrane helices, but these are not supported by any of the other algorithms. We conclude, as proposed previously for the human mitochondrial protoporphyrinogen oxidase (*61*), that human *mito*GlpD is strongly associated with the outer surface of the inner membrane (*14*) but is attached as a peripheral rather than integral membrane protein. A very recent report (*62*) of similar analyses for the yeast *mito*GlpD (Gut2p) also concludes that this protein lacks transmembrane helices. Yeast Gut2p aligns with residues 17−599 of the human *mito*GlpD (full-length precursor sequences; 43% identity), but Gut2p lacks the C-terminal calmodulin homology domain. Janssen et al. (*63*) demonstrated that Gut2p is a peripheral membrane protein that interacts tightly with the mitochondrial inner membrane, which likely is required for its respiratory function. This peripheral localization has been suggested to involve partial insertion of a hydrophobic region as the photoactivatable probe 3-(trifluoromethyl)-3-phenyldiazirine phosphatidylcholine specifically and efficiently labels Gut2p in the mitochondrial inner membrane (*63*).

The properties of the *E. coli* (*16*) and *B. subtilis* (*18*) *bact*GlpDs indicate that their respective membrane associations are considerably weaker, and analysis of the *bact*GlpD sequences with any of the five algorithms described above also fails to identify transmembrane helices. A proposal by Walz et al. (*16*) suggests that the *E. coli* GlpD is a peripheral membrane protein, with residues 355−370 serving as an amphipathic helix that penetrates and stably anchors the protein to the membrane. We now see that the corresponding segment in GlpOΔ is the surface-exposed α9 helix in the FAD-binding domain (Figure 6) that is preceded closely by the loop bearing FAD-binding residues Ile430 and Thr431. This is indeed an amphipathic helix, but the nonpolar side of the helix is buried within the protein core and can in no way interact with the membrane without the domain structure being disrupted. So where might the membrane-anchoring segment reside? We propose that C-terminal helical domain 3 of the GlpDs, which is apparently not involved in catalysis, conveys the peripheral membrane-binding function. The alignment in Figure 6 demonstrates that the respective sequences for the GlpO versus GlpD C-terminal domains are poorly conserved: GlpOΔ aligns with the mature Gut2p (*63*) with 33% identity over the first two domains, but with only 14% identity for the C-terminal segment (GlpOΔ Glu438−Lys607 and Gut2p Glu433−Val612). Also interestingly, the helical structure of the C-terminal domain shows certain similarities with the membrane-binding motif demonstrated for prostaglandin H_2 synthase-1 [Cox-1 (*64*)], a monotopic integral membrane protein. The bulk of the Cox-1 protein faces the lumen of the endoplasmic reticulum, and integration into one leaflet of the membrane occurs via a set of surface helices (the membrane-binding motif). These helices also form the entrance to the narrow channel that leads to the center of the Cox-1 monomer; this arrangement may have functional significance in the delivery of the hydrophobic arachidonic acid substrate from the membrane to the Cox-1 active site. As the *mito*GlpDs reduce membrane-associated quinone substrates, the C-terminal domain in yeast Gut2p might play a role similar to that of Cox-1 in providing access for the hydrophobic GlpD acceptor substrate to the active site. The variability in sequences for the respective C-terminal domains, from the cytosolic GlpO to the tightly bound yeast *mito*GlpD and mammalian enzymes, is expected to provide the structural differentiation required for these distinct electron transfer functions and membrane associations.

Glp Oxidase versus Dehydrogenase Reactivity. Although the GlpDs reduce quinone acceptors (*65*−*67*) instead of molecular oxygen, Mattevi (*68*) has cautioned that there are no structural rules for predicting flavoprotein oxidase versus dehydrogenase function. For example, while the active-site structures of the FMN-containing glycolate oxidase and flavocytochrome b_2 are highly conserved [the two sequences are 37% identical, and a C_α superposition gives a rmsd of 0.93 Å over 311 atoms (*69*)], the relative O_2 reactivities vary by a factor of 10^4−10^5, and the function of the latter enzyme involves one-electron transfers from reduced flavin to heme. Subtle differences in FMN environments (both enzymes also stabilize the FMN-N5−sulfite adduct) have been implicated in this dramatic difference in electron transfer paths from the respective $FMNH_2$, and the specific molecular factors involved in this divergence remain obscure. Similarly, for GlpO versus GlpD, it appears that all of the key residues in the GlpO active site are conserved in GlpD; the goal of gleaning the structural basis for oxidase (O_2) versus dehydrogenase (quinone) functions for GlpO and GlpD remains an elusive one at present.

In *En. casseliflavus* and other lactic acid bacteria capable of growth on glycerol, the genes encoding glycerol kinase [GlpK (*70*)], GlpO, and the glycerol facilitator [GlpF (*71*)] are cotranscribed.[2] An elaborate network of transcriptional as well as post-translational regulatory controls has been described (*72*) which ensures efficient glycerol uptake and catabolism in the absence of phosphotransferase system sugars, and vice versa. The crystal structure of *Streptococcus* sp. GlpO complements and in fact completes the structural picture of this important metabolic network in these heme-deficient bacteria.

ACKNOWLEDGMENT

We thank Dr. Tom Hollis for helpful discussions during final refinements and Dr. Todd Lowther and Dr. Thomas Jonsson for help in data collection.

REFERENCES

1. Green, D. E. (1936) α-Glycerophosphate dehydrogenase, *Biochem. J. 30*, 629−644.
2. Garrib, A., and McMurray, W. C. (1986) Purification and characterization of glycerol-3-phosphate dehydrogenase (flavin-linked) from rat liver mitochondria, *J. Biol. Chem. 261*, 8042−8048.
3. Brown, L. J., MacDonald, M. J., Lehn, D. A., and Moran, S. M. (1994) Sequence of rat mitochondrial glycerol-3-phosphate dehydrogenase cDNA. Evidence for EF-hand calcium-binding domains, *J. Biol. Chem. 269*, 14363−14366.
4. MacDonald, M. J., and Brown, L. J. (1996) Calcium activation of mitochondrial glycerol phosphate dehydrogenase restudied, *Arch. Biochem. Biophys. 326*, 79−84.
5. Austin, D., and Larson, T. J. (1991) Nucleotide sequence of the *glpD* gene encoding aerobic *sn*-glycerol 3-phosphate dehydrogenase of *Escherichia coli* K-12, *J. Bacteriol. 173*, 101−107.
6. Holmberg, C., Beijer, L., Rutberg, B., and Rutberg, L. (1990) Glycerol catabolism in *Bacillus subtilis*: Nucleotide sequence of the genes encoding glycerol kinase (*glpK*) and glycerol-3-phosphate dehydrogenase (*glpD*), *J. Gen. Microbiol. 136*, 2367−2375.
7. Esders, T. W., and Michrina, C. A. (1979) Purification and properties of L-α-glycerophosphate oxidase from *Streptococcus faecium* ATCC 12755, *J. Biol. Chem. 254*, 2710−2715.
8. Claiborne, A. (1986) Studies on the structure and mechanism of *Streptococcus faecium* L-α-glycerophosphate oxidase, *J. Biol. Chem. 261*, 14398−14407.
9. Parsonage, D., Luba, J., Mallett, T. C., and Claiborne, A. (1998) The soluble α-glycerophosphate oxidase from *Enterococcus casseliflavus*. Sequence homology with the membrane-associated dehydrogenase and kinetic analysis of the recombinant enzyme, *J. Biol. Chem. 273*, 23812−23822.
10. Bender, K., Newsholme, P., Brennan, L., and Maechler, P. (2006) The importance of redox shuttles to pancreatic β-cell energy metabolism and function, *Biochem. Soc. Trans. 34*, 811−814.
11. Ravier, M. A., Eto, K., Jonkers, F. C., Nenquin, M., Kadowaki, T., and Henquin, J. C. (2000) The oscillatory behavior of pancreatic islets from mice with mitochondrial glycerol-3-phosphate dehydrogenase knockout, *J. Biol. Chem. 275*, 1587−1593.
12. Eto, K., Tsubamoto, Y., Terauchi, Y., Sugiyama, T., Kishimoto, T., Takahashi, N., Yamauchi, N., Kubota, N., Murayama, S., Aizawa, T., Akanuma, Y., Aizawa, S., Kasai, H., Yazaki, Y., and Kadowaki, T. (1999) Role of NADH shuttle system in glucose-induced activation of mitochondrial metabolism and insulin secretion, *Science 283*, 981−985.

[2] D. Parsonage and A. Claiborne, unpublished experiments.

13. Cole, E. S., Lepp, C. A., Holohan, P. D., and Fondy, T. P. (1978) Isolation and characterization of flavin-linked glycerol-3-phosphate dehydrogenase from rabbit skeletal muscle mitochondria and comparison with the enzyme from rabbit brain, *J. Biol. Chem. 253*, 7952−7959.
14. Klingenberg, M. (1970) Localization of the glycerol-phosphate dehydrogenase in the outer phase of the mitochondrial inner membrane, *Eur. J. Biochem. 13*, 247−252.
15. Schryvers, A., Lohmeier, E., and Weiner, J. H. (1978) Chemical and functional properties of the native and reconstituted forms of the membrane-bound, aerobic glycerol-3-phosphate dehydrogenase of *Escherichia coli*, *J. Biol. Chem. 253*, 783−788.
16. Walz, A. C., Demel, R. A., de Kruijff, B., and Mutzel, R. (2002) Aerobic *sn*-glycerol-3-phosphate dehydrogenase from *Escherichia coli* binds to the cytoplasmic membrane through an amphipathic α-helix, *Biochem. J. 365*, 471−479.
17. Yeh, J. I., Du, S., Tortajada, A., Paulo, J., and Zhang, S. (2005) Peptergents: Peptide detergents that improve stability and functionality of a membrane protein, glycerol-3-phosphate dehydrogenase, *Biochemistry 44*, 16912−16919.
18. Hedin, T. (1991) Glycerol-3-phosphate dehydrogenase of *Bacillus subtilis* BR95: Cellular localisation, biochemical properties and reconstitution into natural and artificial membranes, Master's Thesis, University of Lund, Lund, Sweden.
19. Koditschek, L. K., and Umbreit, W. W. (1969) α-Glycerophosphate oxidase in *Streptococcus faecium* F 24, *J. Bacteriol. 98*, 1063−1068.
20. Charrier, V., Luba, J., Parsonage, D., and Claiborne, A. (2000) Limited proteolysis as a structural probe of the soluble α-glycerophosphate oxidase from *Streptococcus* sp., *Biochemistry 39*, 5035−5044.
21. Finnerty, C. M., Charrier, V., Claiborne, A., and Karplus, P. A. (2002) Crystallization and preliminary crystallographic analysis of the soluble α-glycerophosphate oxidase from *Streptococcus* sp., *Acta Crystallogr. D58*, 165−166.
22. Nicely, N. I., Parsonage, D., Paige, C., Newton, G. L., Fahey, R. C., Leonardi, R., Jackowski, S., Mallett, T. C., and Claiborne, A. (2007) Structure of the type III pantothenate kinase from *Bacillus anthracis* at 2.0 Å resolution: Implications for coenzyme A-dependent redox biology, *Biochemistry 46*, 3234−3245.
23. Cornish-Bowden, A. (1995) *Fundamentals of Enzyme Kinetics*, Portland Press Ltd., London.
24. Pflugrath, J. W. (1999) The finer things in X-ray diffraction data collection, *Acta Crystallogr. D55*, 1718−1725.
25. Terwilliger, T. C., and Berendzen, J. (1999) Automated MAD and MIR structure solution, *Acta Crystallogr. D55*, 849−861.
26. Terwilliger, T. C. (2000) Maximum-likelihood density modification, *Acta Crystallogr. D56*, 965−972.
27. Terwilliger, T. C. (2003) Automated main-chain model building by template matching and iterative fragment extension, *Acta Crystallogr. D59*, 38−44.
28. Murshudov, G. N., Vagin, A. A., and Dodson, E. J. (1997) Refinement of macromolecular structures by the maximum-likelihood method, *Acta Crystallogr. D53*, 240−255.
29. Emsley, P., and Cowtan, K. (2004) Coot: Model-building tools for molecular graphics, *Acta Crystallogr. D60*, 2126−2132.
30. Brunger, A. T., Adams, P. D., Clore, G. M., DeLano, W. L., Gros, P., Grosse-Kunstleve, R. W., Jiang, J. S., Kuszewski, J., Nilges, M., Pannu, N. S., Read, R. J., Rice, L. M., Simonson, T., and Warren, G. L. (1998) Crystallography & NMR system: A new software suite for macromolecular structure determination, *Acta Crystallogr. D54*, 905−921.
31. Storoni, L. C., McCoy, A. J., and Read, R. J. (2004) Likelihood-enhanced fast rotation functions, *Acta Crystallogr. D60*, 432−438.
32. Read, R. J. (2001) Pushing the boundaries of molecular replacement with maximum likelihood, *Acta Crystallogr. D57*, 1373−1382.
33. Luzzati, V. (1952) Traitement statistique des erreurs dans la determination des structures cristallines, *Acta Crystallogr. 5*, 802−810.
34. Kabsch, W., and Sander, C. (1983) Dictionary of protein secondary structure: Pattern recognition of hydrogen-bonded and geometrical features, *Biopolymers 22*, 2577−2637.
35. Holm, L., and Sander, C. (1993) Protein structure comparison by alignment of distance matrices, *J. Mol. Biol. 233*, 123−138.
36. Settembre, E. C., Dorrestein, P. C., Park, J. H., Augustine, A. M., Begley, T. P., and Ealick, S. E. (2003) Structural and mechanistic studies on ThiO, a glycine oxidase essential for thiamin biosynthesis in *Bacillus subtilis*, *Biochemistry 42*, 2971−2981.
37. Tsuge, H., Kawakami, R., Sakuraba, H., Ago, H., Miyano, M., Aki, K., Katunuma, N., and Ohshima, T. (2005) Crystal structure of a novel FAD-, FMN-, and ATP-containing L-proline dehydrogenase complex from *Pyrococcus horikoshii*, *J. Biol. Chem. 280*, 31045−31049.
38. Chen, Z. W., Hassan-Abdulah, A., Zhao, G., Jorns, M. S., and Mathews, F. S. (2006) Heterotetrameric sarcosine oxidase: Structure of a diflavin metalloenzyme at 1.85 Å resolution, *J. Mol. Biol. 360*, 1000−1018.
39. Trickey, P., Wagner, M. A., Jorns, M. S., and Mathews, F. S. (1999) Monomeric sarcosine oxidase: Structure of a covalently flavinylated amine oxidizing enzyme, *Structure 7*, 331−345.
40. Mattevi, A., Vanoni, M. A., Todone, F., Rizzi, M., Teplyakov, A., Coda, A., Bolognesi, M., and Curti, B. (1996) Crystal structure of D-amino acid oxidase: A case of active site mirror-image convergent evolution with flavocytochrome b_2, *Proc. Natl. Acad. Sci. U.S.A. 93*, 7496−7501.
41. Dym, O., and Eisenberg, D. (2001) Sequence-structure analysis of FAD-containing proteins, *Protein Sci. 10*, 1712−1728.
42. Lennon, B. W., Williams, C. H., Jr., and Ludwig, M. L. (1999) Crystal structure of reduced thioredoxin reductase from *Escherichia coli*: Structural flexibility in the isoalloxazine ring of the flavin adenine dinucleotide cofactor, *Protein Sci. 8*, 2366−2379.
43. Zhang, W., Zhang, M., Zhu, W., Zhou, Y., Wanduragala, S., Rewinkel, D., Tanner, J. J., and Becker, D. F. (2007) Redox-induced changes in flavin structure and roles of flavin N(5) and the ribityl 2′-OH group in regulating PutA-membrane binding, *Biochemistry 46*, 483−491.
44. Schiffer, A., Fritz, G., Kroneck, P. M., and Ermler, U. (2006) Reaction mechanism of the iron-sulfur flavoenzyme adenosine-5′-phosphosulfate reductase based on the structural characterization of different enzymatic states, *Biochemistry 45*, 2960−2967.
45. Loach, P. A. (1976) Oxidation-reduction potentials, absorbance bands and molar absorbance of compounds used in biochemical studies, in *Handbook of Biochemistry and Molecular Biology* (Fasman, G. D., Ed.) 3rd ed., Vol. I, pp 122−130, CRC Press, Boca Raton, FL.
46. Rossmann, M. G., Moras, D., and Olsen, K. W. (1974) Chemical and biological evolution of nucleotide-binding protein, *Nature 250*, 194−199.
47. Wierenga, R. K., Terpstra, P., and Hol, W. G. J. (1986) Prediction of the occurrence of the ADP-binding $\beta\alpha\beta$-fold in proteins, using an amino acid sequence fingerprint, *J. Mol. Biol. 187*, 101−107.
48. Umhau, S., Pollegioni, L., Molla, G., Diederichs, K., Welte, W., Pilone, M. S., and Ghisla, S. (2000) The X-ray structure of D-amino acid oxidase at very high resolution identifies the chemical mechanism of flavin-dependent substrate dehydrogenation, *Proc. Natl. Acad. Sci. U.S.A. 97*, 12463−12468.
49. Alber, T. C., Davenport, R. C., Jr., Giammona, D. A., Lolis, E., Petsko, G. A., and Ringe, D. (1987) Crystallography and site-directed mutagenesis of yeast triosephosphate isomerase: What can we learn about catalysis from a "simple" enzyme? *Cold Spring Harbor Symp. Quant. Biol. 52*, 603−613.
50. Noble, M. E. M., Wierenga, R. K., Lambeir, A.-M., Opperdoes, F. R., Thunnissen, A.-M. W. H., Kalk, K. H., Groendijk, H., and Hol, W. G. J. (1991) The adaptability of the active site of trypanosomal triosephosphate isomerase as observed in the crystal structures of three different complexes, *Proteins 10*, 50−69.
51. Lloyd, W. J., and Harrison, R. (1974) Interaction of deoxy and deoxyfluoro-substrate analogs and related compounds with *sn*-glycerol-3-phosphate dehydrogenase of locust flight muscle mitochondria, *Arch. Biochem. Biophys. 163*, 185−190.
52. Finn, R. D., Mistry, J., Schuster-Bockler, B., Griffiths-Jones, S., Hollich, V., Lassmann, T., Moxon, S., Marshall, M., Khanna, A., Durbin, R., Eddy, S. R., Sonnhammer, E. L., and Bateman, A. (2006) Pfam: Clans, web tools and services, *Nucleic Acids Res. 34*, D247−D251.
53. Zhao, G., Song, H., Chen, Z. W., Mathews, F. S., and Jorns, M. S. (2002) Monomeric sarcosine oxidase: Role of histidine 269 in catalysis, *Biochemistry 41*, 9751−9764.
54. Zhao, G., and Jorns, M. S. (2005) Ionization of zwitterionic amine substrates bound to monomeric sarcosine oxidase, *Biochemistry 44*, 16866−16874.
55. Choe, J., Guerra, D., Michels, P. A., and Hol, W. G. (2003) *Leishmania mexicana* glycerol-3-phosphate dehydrogenase showed conformational changes upon binding a bi-substrate adduct, *J. Mol. Biol. 329*, 335−349.

56. Ou, X., Ji, C., Han, X., Zhao, X., Li, X., Mao, Y., Wong, L. L., Bartlam, M., and Rao, Z. (2006) Crystal structures of human glycerol 3-phosphate dehydrogenase 1 (GPD1), *J. Mol. Biol. 357*, 858−869.
57. Lehn, D. A., Brown, L. J., Simonson, G. D., Moran, S. M., and MacDonald, M. J. (1994) The sequence of a human mitochondrial glycerol-3-phosphate dehydrogenase-encoding cDNA, *Gene 150*, 417−418.
58. Kall, L., Krogh, A., and Sonnhammer, E. L. (2004) A combined transmembrane topology and signal peptide prediction method, *J. Mol. Biol. 338*, 1027−1036.
59. Zhou, H., Zhang, C., Liu, S., and Zhou, Y. (2005) Web-based toolkits for topology prediction of transmembrane helical proteins, fold recognition, structure and binding scoring, folding-kinetics analysis and comparative analysis of domain combinations, *Nucleic Acids Res. 33*, W193−W197.
60. Juretic, D., Zoranic, L., and Zucic, D. (2002) Basic charge clusters and predictions of membrane protein topology, *J. Chem. Inf. Comput. Sci. 42*, 620−632.
61. Morgan, R. R., Errington, R., and Elder, G. H. (2004) Identification of sequences required for the import of human protoporphyrinogen oxidase to mitochondria, *Biochem. J. 377*, 281−287.
62. Rijken, P. J., De Kruijff, B., and De Kroon, A. I. (2007) Phosphatidylcholine is essential for efficient functioning of the mitochondrial glycerol-3-phosphate dehydrogenase Gut2 in *Saccharomyces cerevisiae*, *Mol. Membr. Biol. 24*, 269−281.
63. Janssen, M. J., van Voorst, F., Ploeger, G. E., Larsen, P. M., Larsen, M. R., de Kroon, A. I., and de Kruijff, B. (2002) Photolabeling identifies an interaction between phosphatidylcholine and glycerol-3-phosphate dehydrogenase (Gut2p) in yeast mitochondria, *Biochemistry 41*, 5702−5711.
64. Picot, D., Loll, P. J., and Garavito, R. M. (1994) The X-ray crystal structure of the membrane protein prostaglandin H2 synthase-1, *Nature 367*, 243−249.
65. Nelson, D. L., and Cox, M. M. (2005) *Lehninger Principles of Biochemistry*, 4th ed., pp 696−716, W. H. Freeman and Company, New York.
66. Bunoust, O., Devin, A., Averet, N., Camougrand, N., and Rigoulet, M. (2005) Competition of electrons to enter the respiratory chain: A new regulatory mechanism of oxidative metabolism in *Saccharomyces cerevisiae*, *J. Biol. Chem. 280*, 3407−3413.
67. Spoering, A. L., Vulic, M., and Lewis, K. (2006) GlpD and PlsB participate in persister cell formation in *Escherichia coli*, *J. Bacteriol. 188*, 5136−5144.
68. Mattevi, A. (2006) To be or not to be an oxidase: Challenging the oxygen reactivity of flavoenzymes, *Trends Biochem. Sci. 31*, 276−283.
69. Lindqvist, Y., Branden, C.-I., Mathews, F. S., and Lederer, F. (1991) Spinach glycolate oxidase and yeast flavocytochrome b_2 are structurally homologous and evolutionarily related enzymes with distinctly different function and flavin mononucleotide binding, *J. Biol. Chem. 266*, 3198−3207.
70. Yeh, J. I., Charrier, V., Paulo, J., Hou, L., Darbon, E., Claiborne, A., Hol, W. G., and Deutscher, J. (2004) Structures of enterococcal glycerol kinase in the absence and presence of glycerol: Correlation of conformation to substrate binding and a mechanism of activation by phosphorylation, *Biochemistry 43*, 362−373.
71. Fu, D., Libson, A., Miercke, L. J., Weitzman, C., Nollert, P., Krucinski, J., and Stroud, R. M. (2000) Structure of a glycerol-conducting channel and the basis for its selectivity, *Science 290*, 481−486.
72. Deutscher, J., Francke, C., and Postma, P. W. (2006) How phosphotransferase system-related protein phosphorylation regulates carbohydrate metabolism in bacteria, *Microbiol. Mol. Biol. Rev. 70*, 939−1031.

BI701685U